Aerosol Science and Technology, 38:833–850, 2004

ISSN: 0278-6826 print / 1521-7388 online
DOI: 10.1080/027868290503082

The Scanning DMA Transfer Function

Don R. Collins,[1] David R. Cocker,[2] Richard C. Flagan,[3] and John H. Seinfeld[3]
[1]*Texas A&M University, Department of Atmospheric Sciences, College Station, Texas*
[2]*University of California, Riverside, Department of Chemical & Environmental Engineering, Riverside, California*
[3]*California Institute of Technology, Department of Chemical Engineering, Pasadena, California*

The scanning differential mobility analyzer (DMA) has been widely employed for measurement of rapidly evolving aerosol size distributions. Interpretation of data from scanning DMAs is greatly facilitated when an exponential voltage ramp is prescribed, since the shape of the instrumental transfer function remains constant throughout a scan. However, that transfer function may differ significantly from that expected for fixed voltage operation. Because no simple analytical description of the scanning DMA transfer function exists, it has been evaluated numerically by simulating particle trajectories within a TSI 3081 cylindrical DMA. These computations yield transfer functions for the DMA up scan that are roughly triangular but with widths significantly greater than those for fixed voltage operation, and transfer functions for the down scan that are highly asymmetric. The impact of these distortions is most obvious when the size distribution of the measured aerosol is narrow, but errors in recovered size and concentration can be significant even when the aerosol size distribution is much broader than the transfer function. The magnitude of these errors is dependent upon the ratio of the mean gas residence time to the exponential voltage time constant, the sheath-to-aerosol-flow ratio, and the technique used to determine the instrument plumbing time. Experimental results for scans across broad and narrow size distributions compare favorably with predictions based on the simulated transfer functions. Simplified corrections are provided that can be used to adjust the concentration and mobility of size distributions recovered using a fixed voltage transfer function.

Received 13 February 2004; accepted 24 June 2004.
We are grateful for support received from the NSF Atmospheric Chemistry and Physical Meteorology Programs through grant ATM-0094342. The authors wish to thank Patrick Chuang and Jian Wang for their assistance during the data collection. We would also like to thank the reviewers of this article for their insightful and extremely helpful suggestions.
Address correspondence to Don R. Collins, Texas A&M University, Department of Atmospheric Sciences, 3150 TAMU, College Station, TX 77843-3150, USA. E-mail: dcollins@tamu.edu

INTRODUCTION

More than 25 years after being developed by Knutson and Whitby (1975), the differential mobility analyzer (DMA) remains one of the primary tools for characterization of submicron aerosol size distributions. Initial applications of the DMA for ambient aerosol measurements was limited to stepping-mode operation (Fissan et al. 1983), in which the applied voltage is incrementally changed and the particle concentration at several discrete sizes is measured. Although the simplicity of this approach may improve measurement accuracy, the time required to measure a complete size distribution in stepping mode is often excessive. In response to the demand to reduce measurement time sufficiently to characterize rapidly evolving size distributions, Wang and Flagan (1990) introduced the scanning electrical mobility spectrometer (SEMS), for which a continuous voltage ramp was employed. This seemingly small modification greatly enhanced the utility of the DMA for ambient aerosol measurements. This voltage-scanning operation was incorporated in the commercial TSI scanning mobility particle sizer (SMPS), and more recently in the MSP scanning mobility spectrometer (SMS).

Regardless of how voltage is varied, recovery of an aerosol size distribution from particle counts recorded during a DMA measurement requires a description of the instrument transfer function, which has traditionally been defined as the particle transmission efficiency, Ω, as a function of electrical mobility, Z_p. The fixed voltage DMA transfer function has been explored by a number of groups using a range of analytical and computational techniques. Knutson and Whitby (1975) first determined the theoretical DMA transfer function through analysis of particle stream functions. They showed that, for matched aerosol and sample flow rates, the transfer function is triangular in shape, centered at mobility,

$$Z_p^* = \frac{Q_{sh} \ln \frac{r_2}{r_1}}{2\pi L V}, \qquad [1]$$

with full width at half height,

$$\Delta Z_p = Z_p^* \frac{Q_a}{Q_{sh}}, \quad [2]$$

where Q_{sh} is the sheath flow rate, Q_a is the aerosol flow rate, V is the applied voltage, L is the length of the classification region within the DMA, and r_1 and r_2 are the inner and outer radii of the DMA annulus, respectively. This result is insensitive to the velocity profile within the DMA annulus. Kousaka et al. (1986), Stolzenburg (1988), Zhang and Flagan (1996), and Reischl et al. (1997) evaluated the extent to which the transfer function is broadened due to particle diffusion. More recently, Hagwood et al. (1999) determined the diffusionally broadened transfer function using a Monte Carlo simulation.

Wang and Flagan (1990) recognized that the use of an exponential voltage ramp would facilitate analysis of scanning DMA data since the shape of the transfer function would remain constant throughout a scan. Although they noted that the transfer function shape would be influenced by the gas velocity profile within the annulus, they employed a simplified model that masked these effects. Rather than calculating the actual residence times of particles as they migrate through the classifier, the particle residence time was assumed to be the average of the fluid residence time calculated between the starting and ending radial positions on the particle trajectory. As a result, the scanning DMA transfer function was found to be the same as the fixed voltage transfer function. Efforts to develop more accurate representations for scanning DMAs have included coupling a fixed voltage transfer function with a mathematical description of the transit time between the DMA and detector (Russell et al. 1995), and computing an averaged transfer function for a counting time step (Endo et al. 1997). None of these investigations addressed the potential impact of the voltage ramp on the transfer function shape.

Unlike stepping mode operation in which the mobility of the particles exiting the DMA is the same as that reaching the detector at any measurement time, particles detected during a voltage scan must be related to the paticle mobility exiting the DMA some time earlier. This is most frequently accomplished by shifting the counts array by some specified delay or plumbing time, t_d. Ascribing the correct mobility to a counting interval would ideally be accomplished by first calculating the mobility of the particles exiting as a function of time, and then shifting the counts array by the transit time between the DMA outlet and detection point. The most common approach for calculating the particle mobility exiting the DMA is substitution of the average voltage applied during the particle residence time for V in Equation (1). However, it is the electric field experienced by a particle that controls its migration across the DMA annulus, and since that electric field is proportional to $V(t)/r(t)$, the particle trajectory must also be considered. Furthermore, the residence time of a particle is also influenced by the voltage ramp employed since its time-dependent radial velocity will control the amount of time it spends in the low-velocity regions near the walls, and the high-velocity region near the annulus centerline. To simplify the assignment of mobility, the unknown particle residence time is usually replaced by the known mean gas residence time,

$$t_r = \frac{\pi\left(r_2^2 - r_1^2\right)L}{Q_{sh} + Q_a}. \quad [3]$$

The result of these simplifications is that the appropriate plumbing time is, in general, different than the true DMA-detector transit time.

The approach used to determine the plumbing time is typically dependent upon whether data are analyzed from both the up scan (increasing voltage) and down scan (decreasing voltage), or just the up scan. When both up- and down-scan data are analyzed, a plumbing time is usually selected that forces agreement between the recovered up- and down-scan distributions. For the analysis provided here, this approach will be referred to as up-down agreement (UDA). When data are recorded only during the up scan, as with the TSI SMPS systems, the plumbing time is either determined by directly measuring the transit time between the DMA and detector (here referred to as the TT approach), or by injecting particles of known size such as polystyrene latex and choosing a plumbing time that shifts the peak in the recovered distribution to the expected size (here referred to as PSL). In general, the plumbing time calculated through each of these approaches is different.

The voltage applied to a scanning DMA is varied exponentially, with time constant

$$\tau_v = \frac{t_s}{\ln \frac{V_{\max}}{V_{\min}}}, \quad [4]$$

where t_s is the scan time, and $V_{\min}$ and $V_{\max}$ are the lower and upper limits of the voltage ramp, respectively. When τ_v is much greater than t_r, the voltage an individual particle experiences is nearly constant, and little difference is expected between the scanning and fixed voltage transfer functions. As the ratio of t_r to τ_v increases, particle trajectories begin to deviate from those within a fixed voltage DMA. Because of the repeated use of the t_r-to-τ_v, ratio, it will be referred to as $\tilde{t}_r$ in the discussion that follows. Figure 1 shows the trajectories of sampled particles beginning and ending at the same radial positions, but experiencing different voltage profiles along the way. The impact of these altered trajectories on the DMA transfer function is not easily determined, which is one of the reasons the fixed voltage description has been frequently substituted.

As computer control of flow rates and voltage improved the precision of DMA measurements, persistent biases in recovered distributions were observed. Specifically, unexplained differences between the concentrations measured during the up and down scan have been observed in data collected using multiple instruments. Figure 2 shows the results of a series of laboratory measurements aimed at characterizing this bias. The ammonium

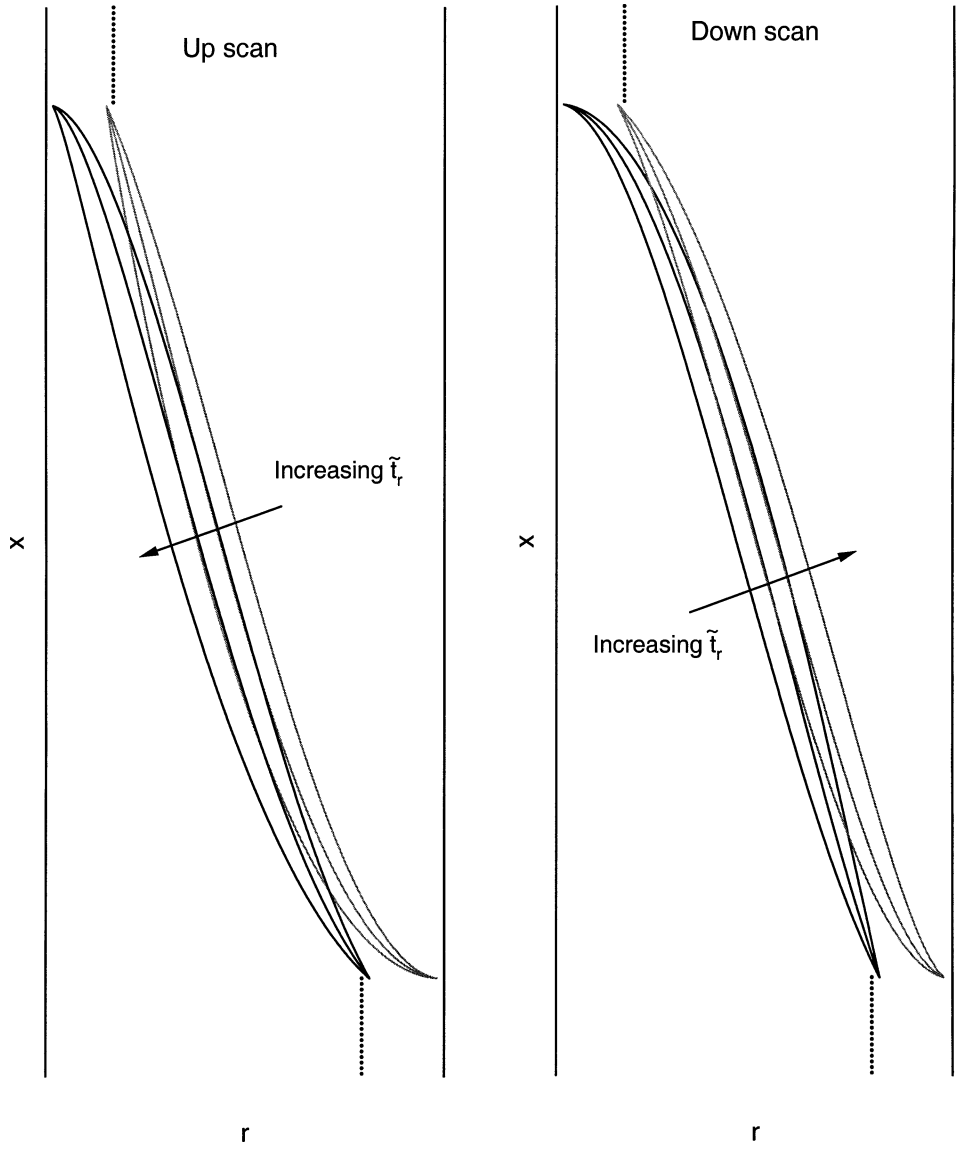

Figure 1. Simulated particle trajectories within the DMA showing the influence of voltage scanning. The dotted lines near the top and bottom of the figures represent the boundaries of the aerosol and sample flows, respectively.

sulfate aerosol analyzed was generated using an atomizer and injected into a 60 m^3 Teflon chamber typically used for smog chamber studies. The chamber was used for this experiment to minimize fluctuations in aerosol concentration. For each of these measurements, the voltage applied to a TSI 3081 DMA was ramped between 10 and 10000 V, while the sheath and sample flows were fixed at 2.5 and 0.25 l/min, respectively. Although the bias was most pronounced for short scan times, the concentration measured during the up scan was still 3% higher than that measured during the down scan for the longest scan time considered (200 s). Attempts to explain the observed differences as the result of increased losses during the down scan were unsuccessful. It will be demonstrated that this bias is dependent upon $\tilde{t}_r$, which suggests it will be most pronounced during measurement of large particles since long residence times are needed to allow the low mobility particles to migrate between the DMA electrodes. Therefore, DMAs used primarily for measurement of small particles such as the TSI radial and nano DMAs will not be considered here. Other DMAs commonly used to measure larger particles such as the Aerosol Dynamics high-flow DMA (HF-DMA; Stolzenburg et al. 1998), and the Vienna-type DMA (Winklmayr et al. 1991) will also not be evaluated here.

SIMULATION DETAILS

Following the approach taken by Hagwood et al. (1999) to determine the diffusionally broadened transfer function at fixed

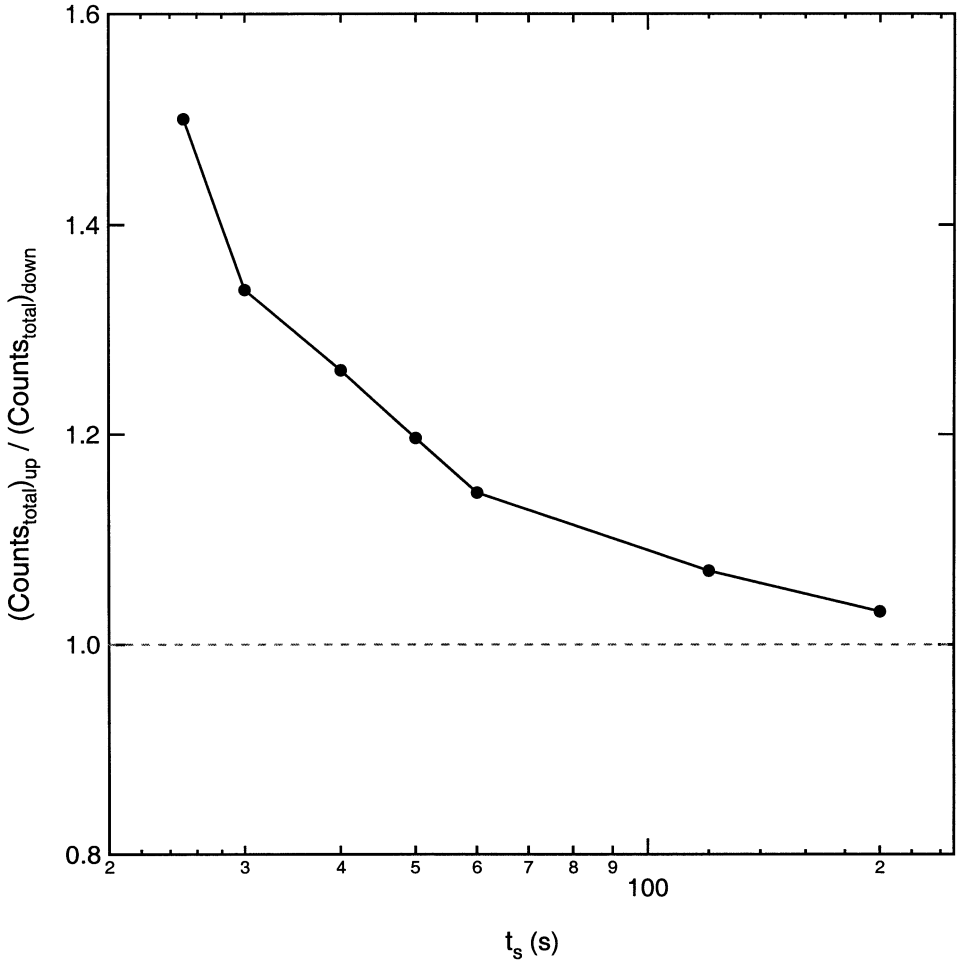

Figure 2. Experimentally observed concentration bias between up- and down-scan measurements with a TSI 3081 DMA. Sheath and aerosol flow rates were fixed at 2.5 and 0.25 l/min, respectively, and the voltage was ramped between 10 and 10000 V. The ammonium sulfate aerosol analyzed was generated with an atomizer and injected into a 60 m^3 Teflon chamber to minimize fluctuations in concentration.

voltage, the scanning DMA transfer function was investigated by employing a particle trajectory-based simulation. For the cylindrical geometry DMA considered here, a particle possessing a charge of the appropriate polarity has velocities in the x and r directions of

$$\frac{dx}{dt} = u(r), \quad [5]$$

$$\frac{dr}{dt} = Z_p E(r) = \frac{Z_p V}{r \ln(r_1/r_2)}, \quad [6]$$

where $u(r)$ and $E(r)$ are the mean gas velocity and electric field at radial position r, respectively. The flow between the concentric cylinders is assumed to be fully developed. The impact of deviations from this idealized velocity profile such as those described by Eichler et al. (1998), Chen et al. (1999), and Collins et al. (2000) is neglected in this analysis. To evaluate the transfer function, 50 particles of equal mobility are introduced across the aerosol flow at each 0.005 s integration time step. The spacing of the injection radii is inversely related to the product of the radius and the gas velocity, so that each particle represents an equal portion of the total aerosol flow. The position of each of the introduced particles is tracked through the DMA and the number exiting with the sample flow during a 0.2 s time interval is used to calculate the value of the transfer function at the specified mobility. The simulation is then repeated over the mobility range for which the transfer function is nonzero. The number of particles injected, the integration time step, the counting time interval, and the mobility resolution were chosen to balance the accuracy of the resulting simulated transfer function with the time needed to complete a simulation. Details of the DMA dimensions and scan parameters used for most of the analyses described below are provided in Table 1. Although the influence of particle diffusion has been simulated using this model, the results will

Table 1
Details of the DMA and simulation parameters

DMA Geometry	Cylindrical
Length (cm)	44.44
Inner radius (cm)	0.937
Outer radius (cm)	1.958
Sheath and excess flow rates (l/min)	2.5
Aerosol and sample flow rates (l/min)	0.25
Mean gas residence time (s)	9.00
Minimum applied voltage	10
Maximum applied voltage	10000

not be considered here since it would be necessary to describe multiple transfer functions for a given set of scan parameters as the variation in particle size throughout a scan translates into a variation in particle diffusivity. The transfer function simulated in this way describes the ratio of the rate at which particles of specified mobility exit in the sample flow to the rate at which they enter in the aerosol flow.

RESULTS

Scanning DMA Transfer Functions

Scanning DMA transfer functions were evaluated for 16 different scan times ranging from 20 s to 1 h ($3.11 \geq \tilde{t}_r \geq 0.0173$). To show the differences between the up- and down-scan transfer functions more clearly, they were shifted logarithmically in opposite directions until roughly lining up. This shift, which is depicted in Figure 3 for a 45 s scan time, is equivalent to the impact of adjusting the plumbing time to force agreement of distributions recovered during up and down scans. Much of the initial separation between the two transfer functions shown in Figure 3a is caused by the substitution of the mean gas flow residence time for the true particle residence time. Figure 4 shows 12 sets of transfer functions along with the fixed-voltage triangular transfer function for reference. As is evident from the 3600 s scan time ($\tilde{t}_r = 0.0173$) simulation, for very small $\tilde{t}_r$ the scanning DMA transfer function is nearly identical to that for fixed-voltage operation. With increasing $\tilde{t}_r$, obvious differences between the simulated transfer function and that for fixed-voltage operation develop. The up-scan transfer function retains a roughly triangular shape, although instrument resolution, $\mathcal{R} = Z_p^*/\Delta Z_p$ (Zhang

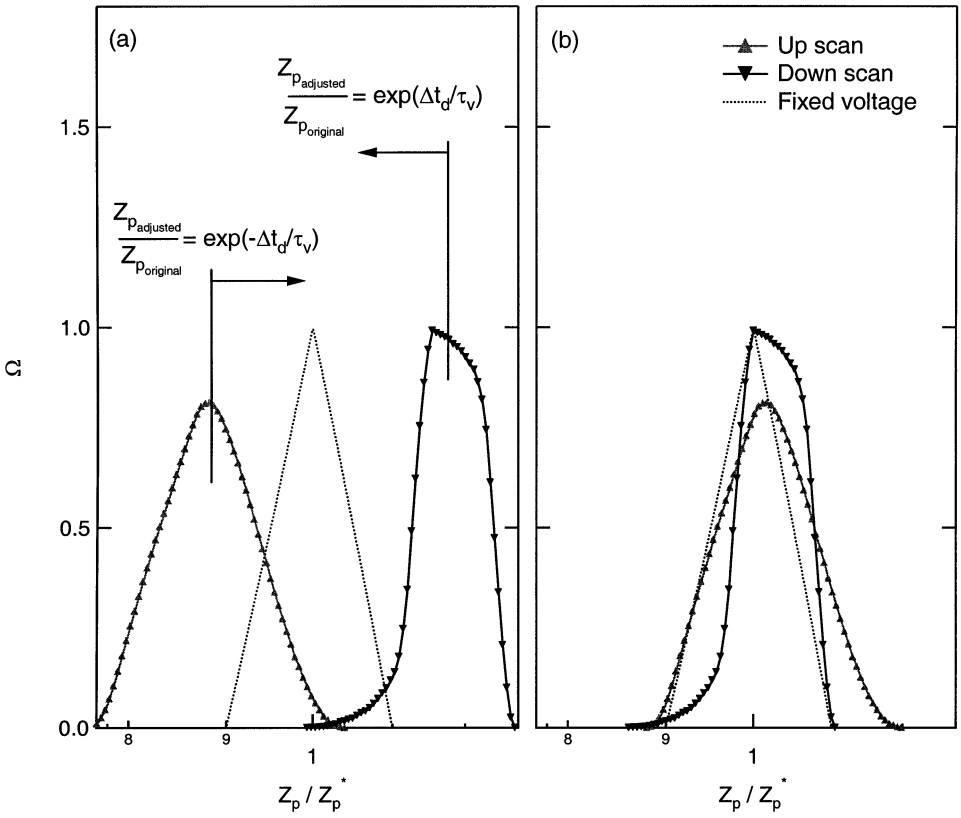

Figure 3. Simulated transfer functions for $t_s = 45$ s ($\tilde{t}_r = 1.38$). (a) The transfer functions were calculated assuming the particle residence time was equal to the mean gas flow residence time. (b) The transfer functions were shifted logarithmically in opposite directions as would be done when a plumbing time is chosen to force agreement between distributions recovered during up and down scans. The triangular transfer function expected for fixed voltage operation is shown for reference. Equation (1) was used to calculate Z_p^*.

and Flagan 1996), is below that expected for a fixed-voltage DMA, as shown in Figure 5. For reference, the resolution for $t_s = 60$ s ($\tilde{t}_r = 1.04$) is equivalent to that of the diffusionally broadened transfer function for 35 nm particles classified with a DMA operated with the same flow rates at 298 K, 1013 hPa (calculated using Stolzenburg 1988). The down-scan transfer functions exhibit an even greater degree of distortion. For comparison with the up scan results, the resolution calculated for the down-scan transfer functions is also included in Figure 5. Unlike the up-scan transfer functions, those of the down scans are asymmetrical, with a shape that varies from nearly triangular for $t_s \geq 600$ s ($\tilde{t}_r \leq 0.104$) to almost rectangular for $t_s = 60$ s ($\tilde{t}_r = 1.04$). The asymmetry of the down-scan transfer functions becomes pronounced for t_s less than 60 s ($\tilde{t}_r > 1.04$), at

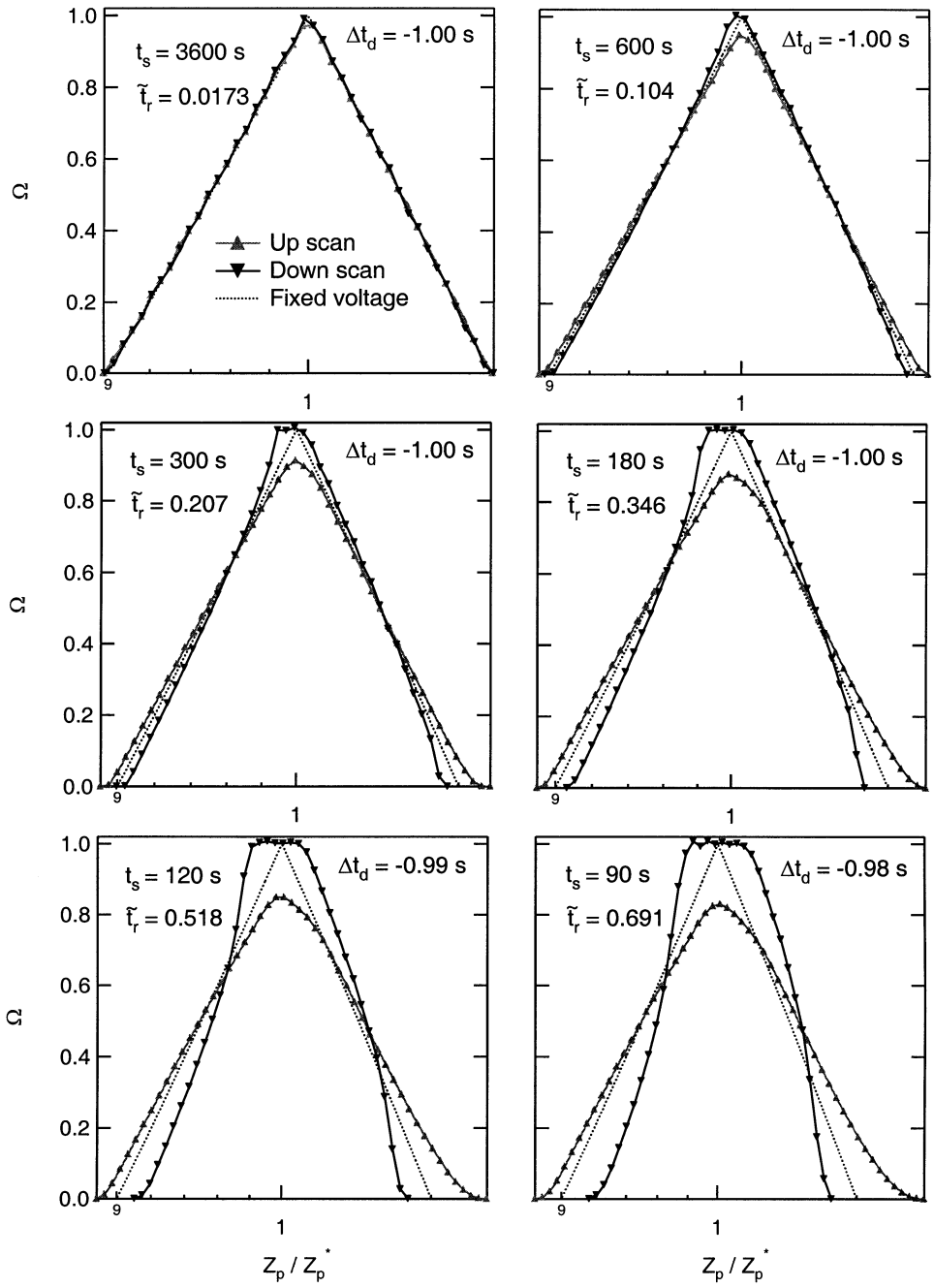

Figure 4. Simulated scanning DMA transfer functions. The up- and down-scan transfer functions were logarithmically shifted in opposite directions according to the expressions included in Figure 3. The triangular transfer function expected for fixed voltage operation is shown for reference. Equation (1) was used to calculate Z_p^*. *(Continued)*

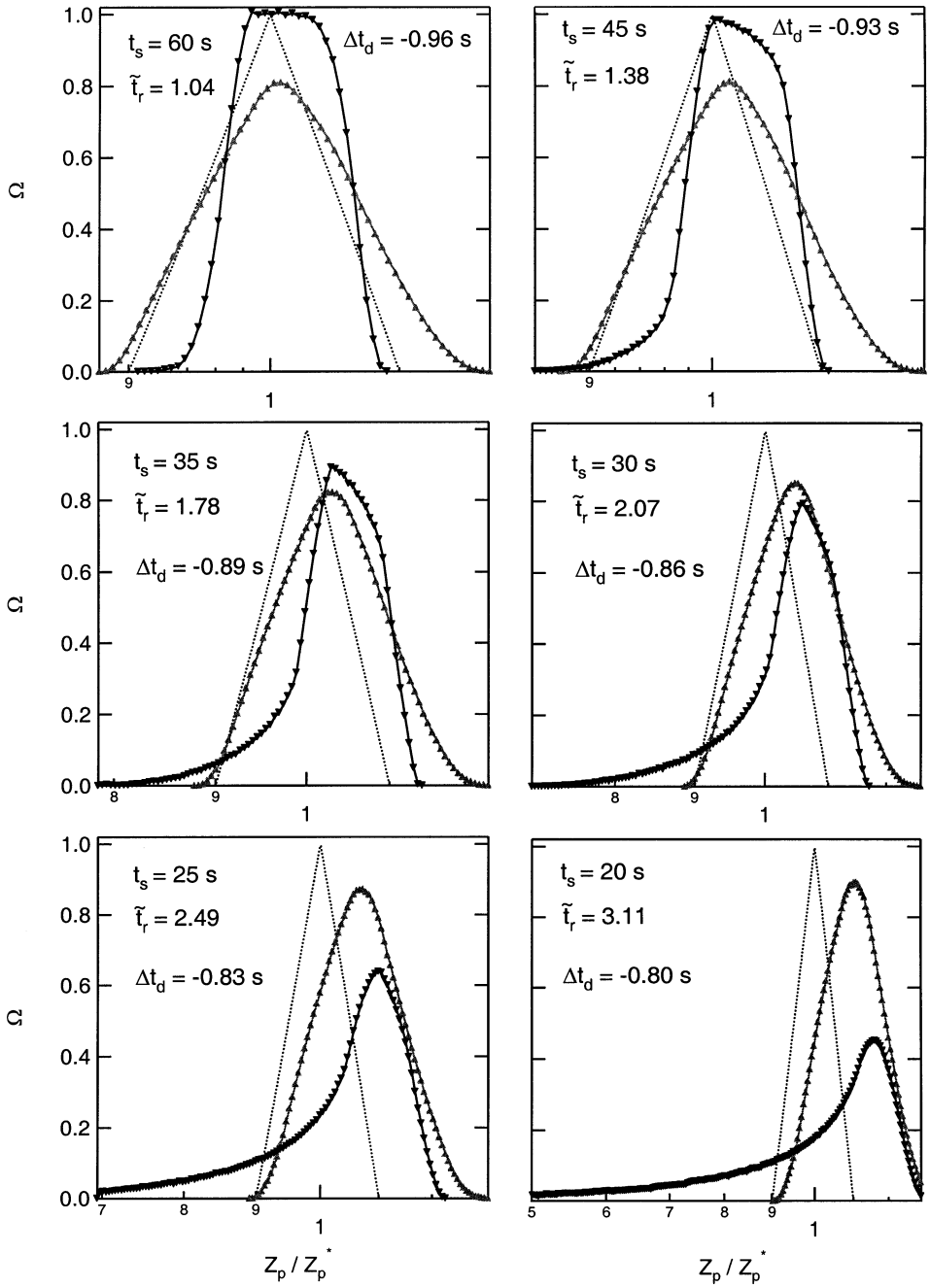

Figure 4. (Continued.)

which point an elongated tail on the low mobility side develops. Although $\mathcal{R}$ is generally greater for the down-scan transfer functions, the suitability of this parameter is questionable for such irregular shapes.

The distortion of the transfer function shape is the most obvious influence of voltage scanning. However, the transfer function shape will influence measurements only when the width of the size distribution of interest is comparable to or less than that of the transfer function. For broad aerosol size distributions, it is the more subtle differences between the scanning-voltage and fixed-voltage transfer functions that will impact the recovered distributions. Specifically, the area beneath the transfer functions is variable, and, after being shifted to line up, the scanning DMA transfer functions are centered at a higher mobility than the ideal triangular transfer function. The displacement in mobility from the expected position of the ideal transfer function can translate into an incorrect assignment of particle size, while the differences in area can cause errors in recovered concentration.

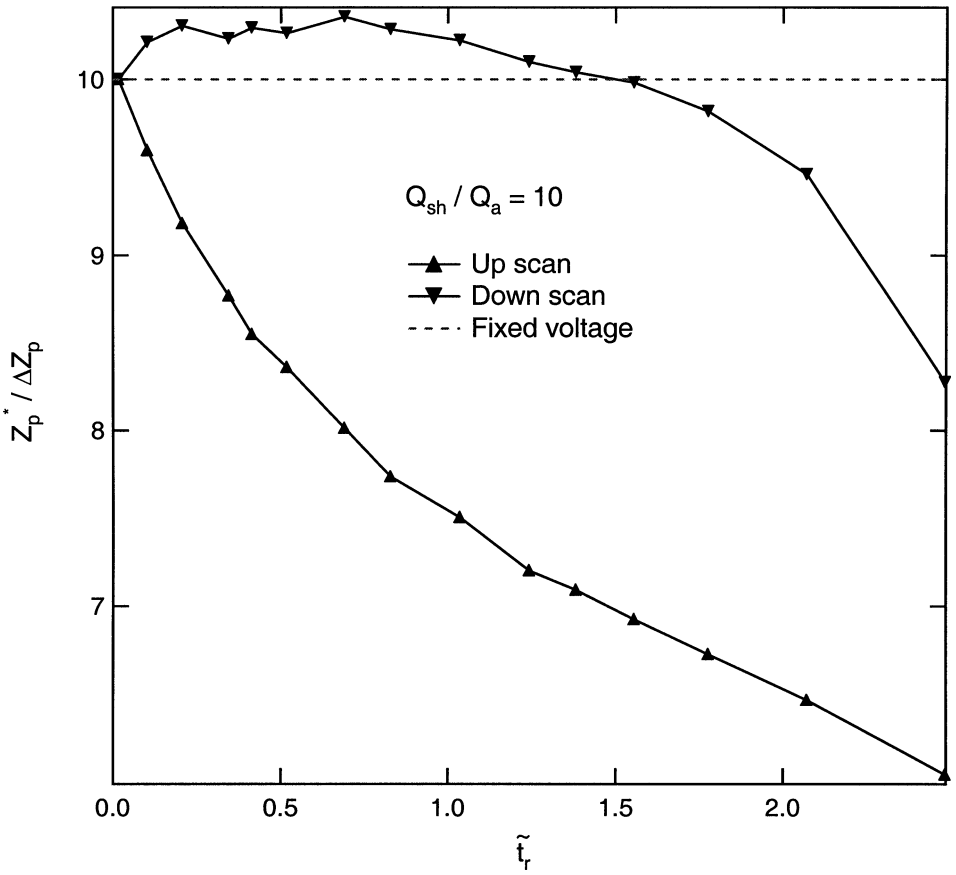

Figure 5. Simulated resolution, $\mathcal{R} = Z_p^*/\Delta Z_p$, of the scanning DMA. The spacing between consecutive mobilities used in the simulations limits the smoothness of the curves.

The same voltage range and flow rates were used to simulate all of the transfer functions shown in Figure 4. Since few operators will use these exact ramp parameters, it is most convenient to consider $\tilde{t}_r$ rather than t_s. Particle trajectories for a given $\tilde{t}_r$ are fixed, so it is expected that the resulting transfer functions will be equivalent as well. This is shown to be true in Figure 6, which presents three different sets of transfer functions calculated for a DMA operated with $\tilde{t}_r = 2.07$. These transfer functions were not shifted like those in Figure 4 to more clearly show the overlap for the different sets of scan parameters.

Experimental Verification

As a first test of the accuracy of the simulated transfer functions, their impact on the recovery of a broad aerosol size distribution such as that which produced the data shown in Figure 2 is considered. The simulated transfer functions were used to generate DMA response matrices for a scan with 200 counting intervals. For example, a counting time step, t_c, of 0.3 s was used for the 60 s scan. The response matrices included aerosol charging probability (Wiedensohler 1988), while the counting efficiency of the TSI 3010 condensation particle counter (CPC) used during the experiment was assumed to be 1.0 because the particles measured were much larger than its detection limit. The expected particle counts were calculated by simulating a scan across a log-normal size distribution having a mean diameter of 0.08 μm and a geometric standard deviation of 1.2. The mean diameter was chosen since it corresponds roughly to the particle size measured half way through the 10–10000 V voltage ramp, and the standard deviation was chosen to ensure that the width of the distribution is significantly greater than that of any of the transfer functions but still narrow enough to be completely captured during the scan. Figure 7 shows the comparison between the predicted ratio of particles counted during the up and down scans, and that measured. The experimentally observed dependence of the counts bias on $\tilde{t}_r$ is captured in the simulated results. The slopes of the measured and predicted curves are approximately the same, and both approach 1.0 for small $\tilde{t}_r$. The small discrepancy between the measured and simulated results is likely the result of neglect within the simulation of nonidealities in the electric and flow fields within the DMA.

For the broad aerosol size distributions analyzed in the smog chamber experiment, the influence of voltage scanning was largely limited to changes in recovered concentration due to differences in the area beneath the transfer functions. As the width of the transfer function approaches that of the measured aerosol

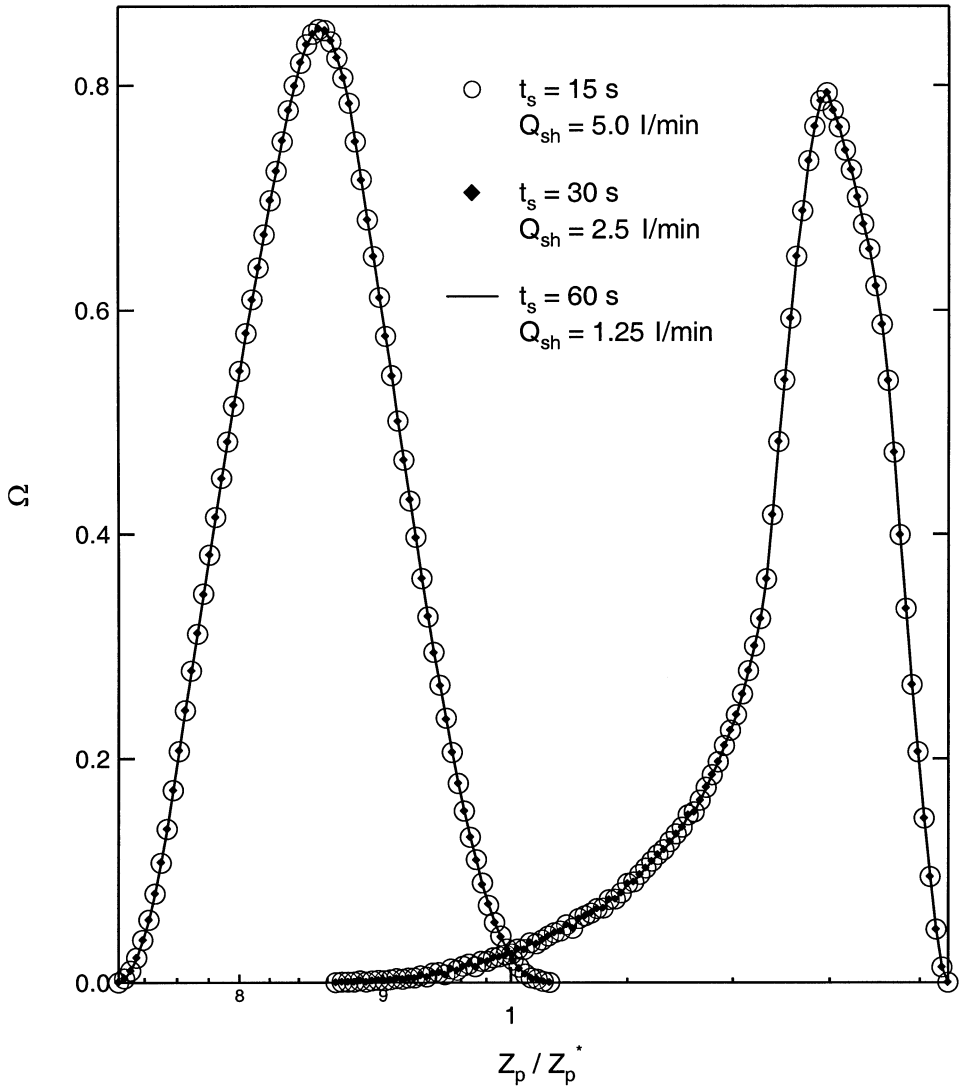

Figure 6. Demonstration of the dependence of transfer function shape on $\tilde{t}_r = t_r/\tau_v$. The three ramps considered have the same $\tilde{t}_r$, which results in identical transfer functions. The transfer functions were not shifted like those shown in Figure 4 in order to more clearly show the overlap for the different sets of ramp parameters.

size distribution, the recovered distribution begins to reflect the shape of the transfer function. Were a truly monodisperse aerosol analyzed, the shape of the recovered distribution would be nearly identical to that of the transfer function. To further validate the simulated transfer functions, a TSI 3081 was used to analyze Interfacial Dynamics, Inc. 0.06 μm polystyrene latex particles that were generated with an atomizer and separated using another DMA operated at fixed voltage. A TSI 3025 CPC was used to detect the classified aerosol since its low mixing time constant minimizes smearing of the recovered distribution during rapid scans (Russell et al. 1995; Collins et al. 2002). The experimental counting time interval used was chosen to provide adequate counting statistics. Multiple scans for each set of ramp parameters were combined to further improve counting statistics and reduce the impact of variations in the atomizer output. For all of the measurements, the sheath and sample flow rates were controlled to 2.5 and 0.25 l/min, respectively, and the voltage was ramped from 5 to 5000 V.

The counting intervals used in the simulations were less than those used in the experiment in order to provide greater resolution for the predicted distributions. Both sets of counting intervals are provided in Table 2. As was done for the comparison with the broad size distribution measurements, the simulated counts were determined by scanning across a single log-normal distribution. For this comparison, a mean diameter of 0.06 μm and a geometric standard deviation of 1.035 were used. Although there is substantially less mixing within the TSI 3025 CPC than most other CPCs, the rapid scans across such a narrow distribution resulted in some smearing of the distributions. Rather than attempting to adjust the experimental data, the impact of the

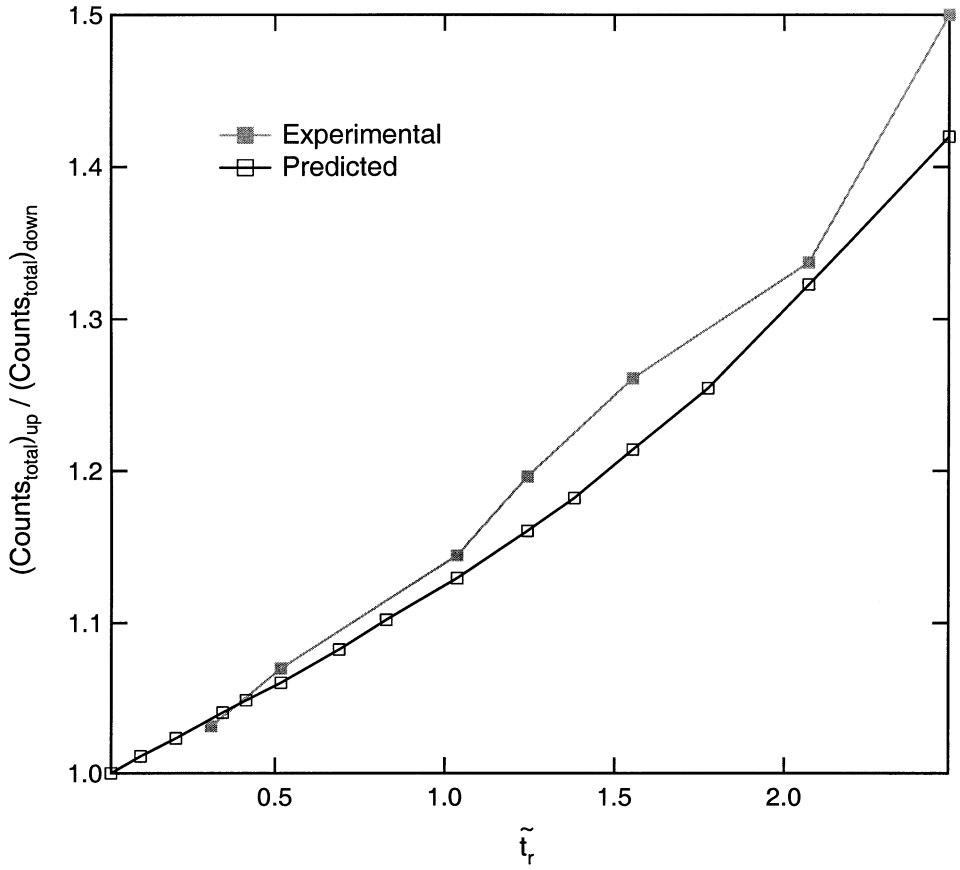

Figure 7. Comparison of the simulated and experimentally observed number concentration bias between up- and down-scan measurements.

smearing was included in the simulation. An exponential time constant of 0.3 s was used for this comparison, which is greater than the 0.1 s expected for the 3025 because of additional mixing between the outlet of the DMA and the inlet of the CPC. The best fit to the experimental up scans was achieved with a time constant of about 0.4 s, while the best fit to the experimental down scans was achieved with a time constant of about 0.2 s, so the value chosen represents a compromise between the two. The measured and predicted distributions are shown in Figure 8. To facilitate comparison between the results from the six sets of ramp parameters shown, the time during the scan is normalized with respect to the scan time. No attempt to independently adjust the up and down scan counts distributions was made. Therefore, any variability in the aerosol concentration during or between measurements could influence the relative heights of the distributions. The simulation does a good job of capturing the features of the recovered distributions, including the elongated tail predicted in the high $\tilde{t}_r$ down scans. As was true for the comparison with the broad size distribution measurements, there are slight differences between the measured and predicted counts distributions that are at least partially due to deviations between the true gas velocity and electric field profiles and those used in the model. Despite these observed differences, it is clear that the simulation adequately captures the shape and relevant properties of the true scanning DMA transfer functions. For the remainder of this article, only the simulated transfer functions will be considered and no effort to correct or adjust them to match the experimental results will be made. Therefore, it is important to note that while the use of the simulated transfer functions or the parameterizations on which they are based will improve

Table 2
Counting intervals used for comparison with the PSL measurements

t_s(s)	$\tilde{t}_r$	Experimental t_c (s)	Simulation t_c (s)
120	0.518	1	0.5
90	0.691	1	0.2
60	1.04	0.5	0.2
50	1.24	0.5	0.1
40	1.55	0.2	0.1
30	2.07	0.2	0.05
25	2.49	0.1	0.05
20	3.11	0.1	0.05

Data from the 50 and 90 s scans are not shown in Figure 8.

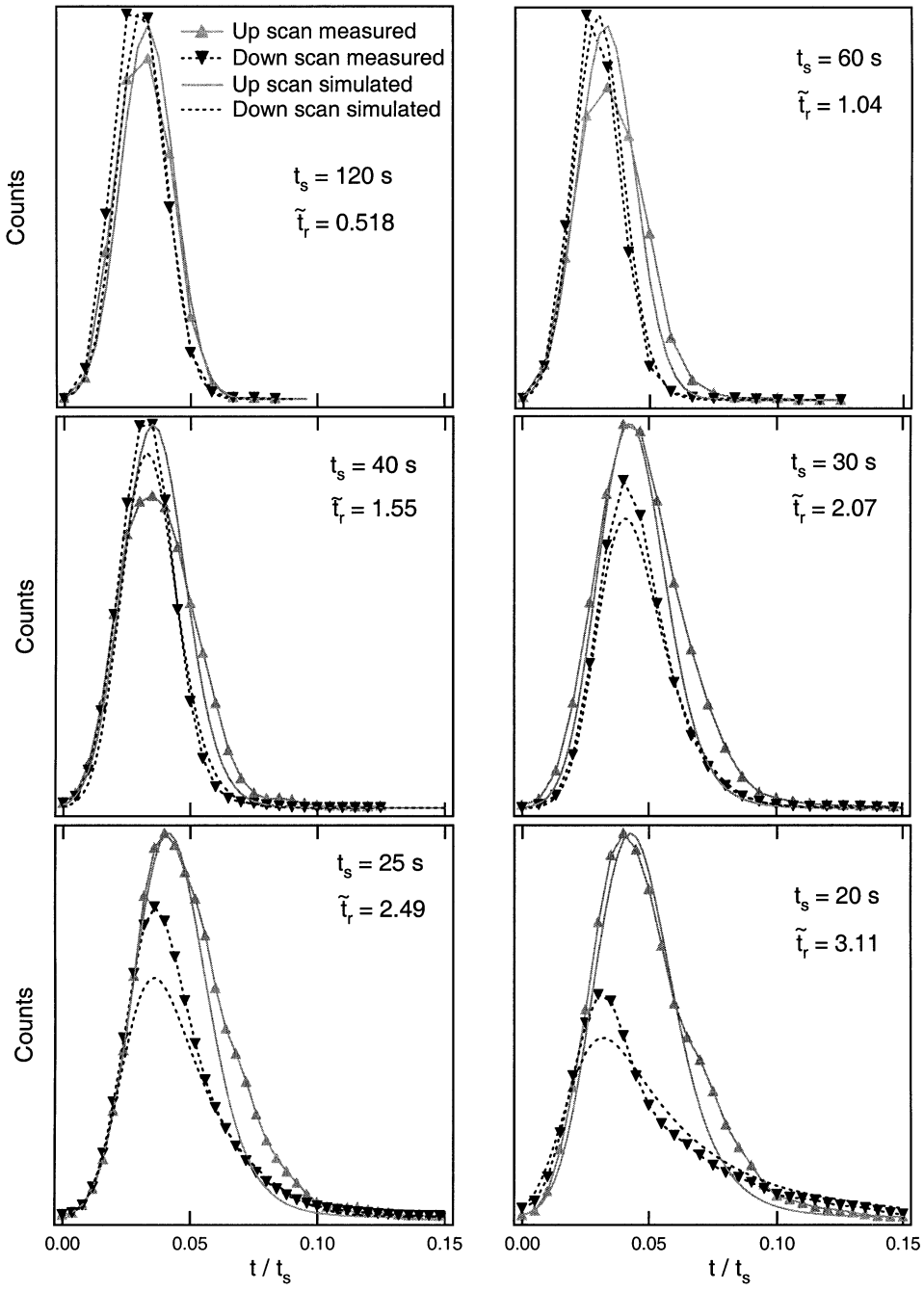

Figure 8. Comparison of the simulated and experimentally observed response of a scanning DMA to a narrow aerosol size distribution.

measurement accuracy, there is still some uncertainty in recovered size and concentration.

Impact of Transfer Function Distortion

To evaluate the impact of the scanning DMA transfer function, the error that results when a fixed voltage transfer function is used in the inversion of data from a scanning DMA was determined. Similar to the approach taken to compare the predicted and measured counts distributions, response matrices based on the simulated transfer functions are created. Simulated counts arrays are generated during a scan across a test-case aerosol size distribution. To relate these particle counts back to a size distribution, additional response matrices are created for which ideal, triangular transfer functions are used. An inversion algorithm (Twomey 1975) is then used to predict the size distribution that would produce the simulated counts array. For

these computations, a log-normal aerosol size distribution with a mean diameter of 0.08 μm and geometric standard deviation of 1.2 was used, although the results were found to be largely insensitive to the size distribution assumed.

The magnitude of the errors in recovered size and concentration are dependent upon the approach taken to determine the instrument plumbing time. For the simulation results described here, particles are assumed to be detected immediately upon exiting the DMA. Therefore, the plumbing time determined using the TT approach would be 0 s. The plumbing time determined using the UDA approach was found just as it would be for an experimental system by iterative adjustment until predicted up- and down-scan distributions agree. The plumbing time used for the PSL approach is dependent upon the scan parameters used during the calibration. For this analysis, it was assumed that the instrument was calibrated during a $t_s = 60$ s scan ($\tilde{t}_r = 1.04$). For each of the three approaches considered, the impact on the recovered number concentration, volume concentration, and mean mobility ($=(\Sigma(Z_p)_i(\Delta N)_i / \Sigma(\Delta N)_i)$ were calculated.

The experimental data that showed the concentration measured during an up scan was consistently higher than that measured during a down scan did not identify which of the two was closer to the true value. The fact that the up-scan transfer function retains a triangular shape, while the down-scan transfer function is greatly distorted, might suggest the down-scan data were erroneous. However, while the concentration recovered assuming a triangular transfer function for both the up and down scan data differ from the true value, Figure 9 shows that the magnitude of the error is far greater for the up-scan data when the UDA approach is used to determine the plumbing time. Errors in recovered volume concentration are larger still. Since up- and down-scan data are often combined into a single distribution, the average number and volume concentrations are shown in the figure as well.

As shown in Figure 4, after the up- and down-scan transfer functions are shifted to line up when the UDA approach is used to determine the plumbing time, they are centered at higher mobility than the ideal triangular transfer function. This causes the recovered distributions to be erroneously shifted to lower mobility if the triangular transfer function is assumed for the inversion. As discussed above, the mobility of particles exiting the DMA at a given time during a scan is estimated using the

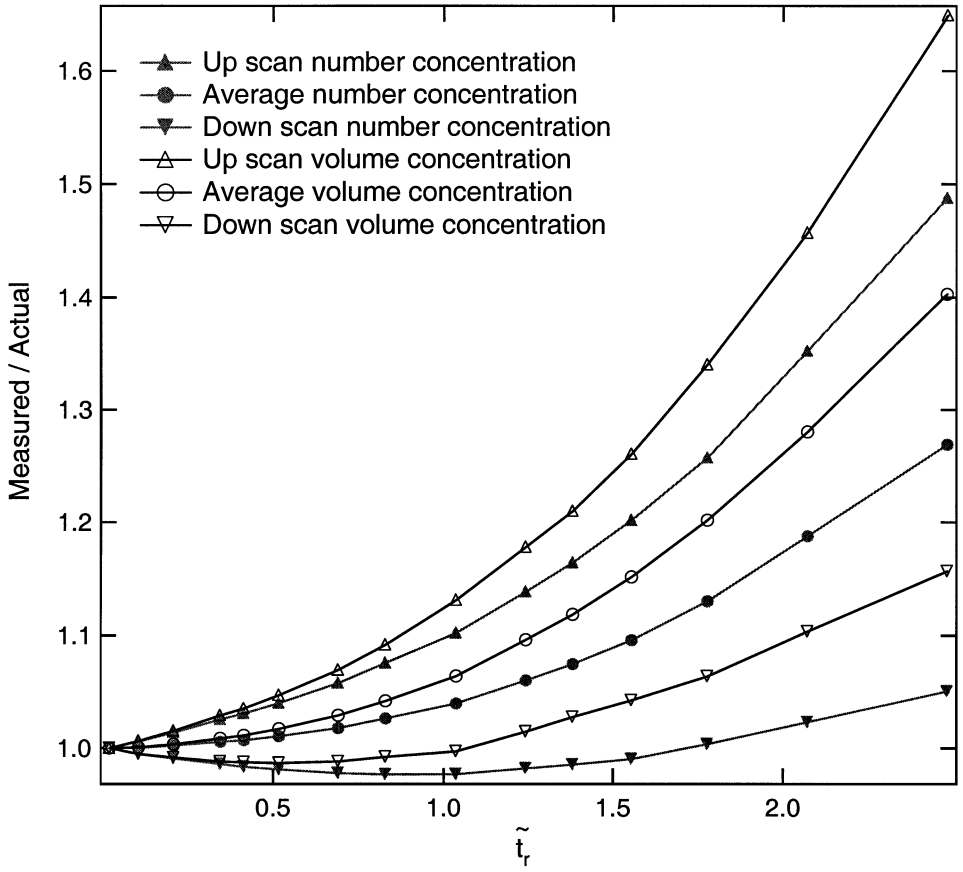

Figure 9. Expected concentration errors in recovered size distributions if the fixed voltage transfer function is used in the data inversion. The plumbing time for each scan time was chosen to force agreement of the mode mobility of the up- and down-scan distributions (UDA approach).

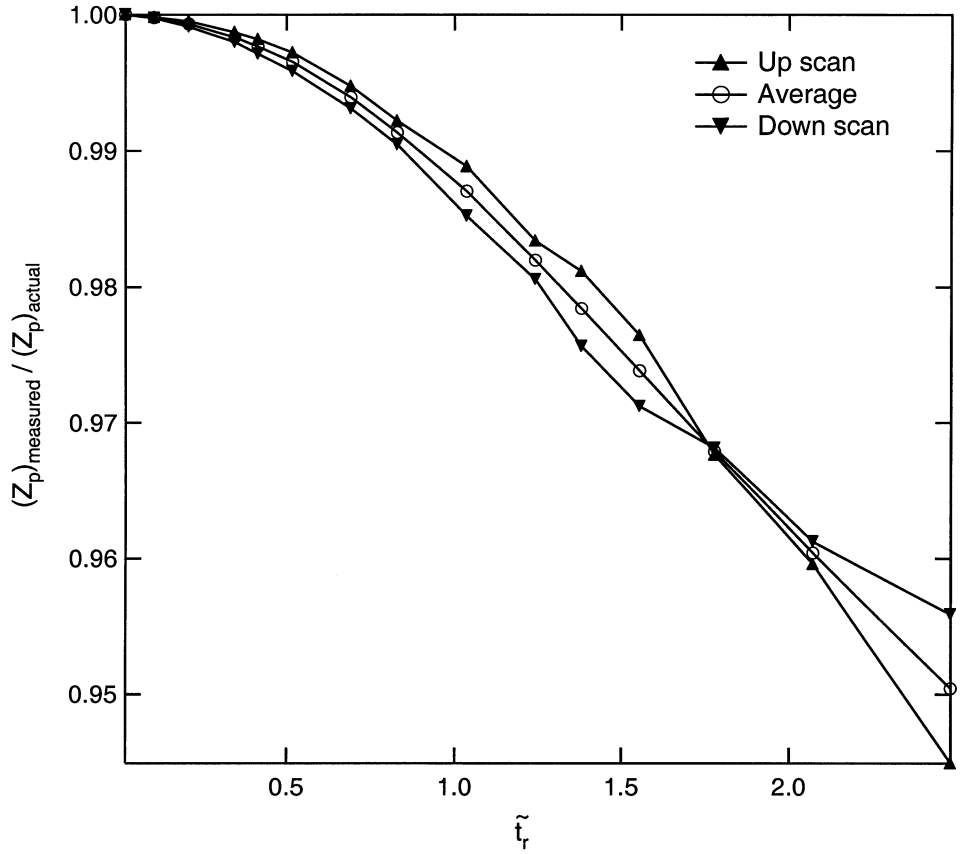

Figure 10. Expected mobility errors in recovered size distributions if the fixed voltage transfer function is used in the data inversion and the UDA approach is used to determine the plumbing time.

average voltage applied over the mean gas residence time. This simplification causes different errors for the up scan and down scan, which is why equal but opposite shifts in mobility through the use of the plumbing time causes the distributions to line up at an incorrect mobility. Therefore, two different plumbing times would have to be used to assign mobility to counts bins correctly. The magnitude of this mobility bias for both the up and down scans is shown in Figure 10. Although the magnitude of this potential error is significantly less than that in recovered concentration, the impact on recovered volume concentrations can be important due to the dependence on the cube of diameter. Since the plumbing time is chosen to force agreement between the up- and down-scan distributions, it is not surprising that the up- and down-scan mean mobilities are very similar. They are not exactly the same only because the mode and mean mobilities differ.

When the true transit time between the DMA outlet and the point of detection (TT approach) is used as the plumbing time, the error in concentration is approximately the same as that for the up scan when the UDA approach is employed. However, since the up- and down-scan distributions are typically averaged when the UDA approach is used, while only the up-scan data are usually considered when the TT approach is used, the concentration bias is greater. Unlike the UDA results, the mean mobility of the recovered distribution is higher than that of the test-case distribution. This is due to the substitution of the gas flow residence time for the typically smaller, but unknown, particle residence time. The combination of increased mobility (and corresponding decreased diameter), and increased concentration, results in a volume concentration bias that is somewhat less than that associated with the UDA approach. The relationship between these potential errors and $\tilde{t}_r$ is shown in Figure 11.

Sizing accuracy is generally greatest when the plumbing time is determined experimentally by injecting particles of a known size (PSL approach). The ramp parameters used during the calibration should be as close as possible to those used during normal operation since they will influence the plumbing time. Although this technique minimizes sizing errors, it is typically used when only the up-scan data are recorded, which results in larger concentration biases. The dependence of the concentration and mean mobility biases on $\tilde{t}_r$ is shown in Figure 12. It is interesting to note that, for many measurement scenarios, the concentration bias associated with the down scan is substantially less than that for the up scan, suggesting that accuracy might be improved by excluding the up scan instead.

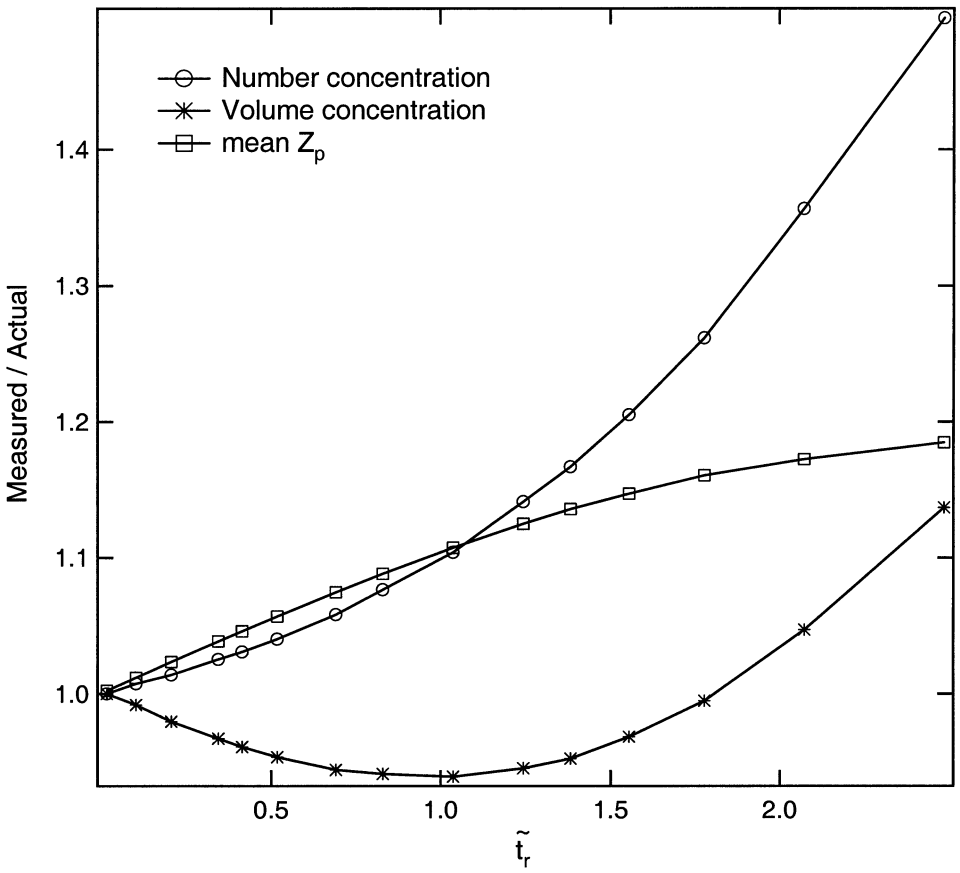

Figure 11. Expected concentration and mobility errors in recovered size distributions if the fixed voltage transfer function is used in the data inversion and the TT approach is used to determine the plumbing time.

Dependence on Q_{sh}/Q_s

A sheath-to-sample flow ratio of 10 was used for the simulated transfer functions described above. Since it is often beneficial to operate at different flow ratios to simplify flow control, maximize count rate, or maximize instrument resolution, the influence of this ratio will be considered. Rather than presenting a complete family of transfer functions and their impacts for a range of flow ratios, only a 60 s scan time will be evaluated. Sample flow rates ranging from 0.025 l/min to 0.5 l/min, corresponding to sheath-to-aerosol flow ratios ranging from 100 to 5, were considered. Deviations between the simulated and actual scanning DMA transfer functions for the high flow ratios are expected to be greater than those for low flow ratios as the impact of flow and electric field nonidealities become more pronounced. The simulated up- and down-scan transfer functions are shown in Figure 13. The up-scan transfer function retains a roughly triangular shape throughout the Q_{sh}/Q_a range considered, while the down-scan transfer functions are again asymmetrical. The classifier resolution, $\mathcal{R}$, of both the up- and down-scan transfer functions is shown in Figure 14. To emphasize the impact of scanning, the $Z_p^*/\Delta Z_p$ ratio is normalized with respect to that for fixed voltage operation at the same flow ratio. Although the theoretical resolution of the scanning DMA does continue to increase with increasing flow ratio, the enhancement is not as large as that for fixed voltage operation. The error in recovered concentration resulting from use of a theoretical triangular transfer function during data inversion is found to increase with increasing Q_{sh}/Q_a, as shown in Figure 15. The error in recovered concentration for the down scan is relatively constant, while that for the up scan increases significantly with increasing sheath-to-aerosol flow ratio.

Simplified Correction

The most accurate method for recovering DMA size distributions is direct use of transfer functions determined for the specific scan parameters employed. Unfortunately, the lack of a simple parameterization to describe the shape of these transfer functions complicates this approach. However, because ambient aerosol size distributions are usually broad relative to the width of these transfer functions, consideration of the exact shape may not be necessary. Instead, the easily described triangular or diffusionally broadened transfer functions can be combined with simple correction factors for mobility and concentration. As with the analyses above, these corrections are based only on the simulated transfer functions, and the influence of nonidealities in the velocity profile and electric field have been neglected.

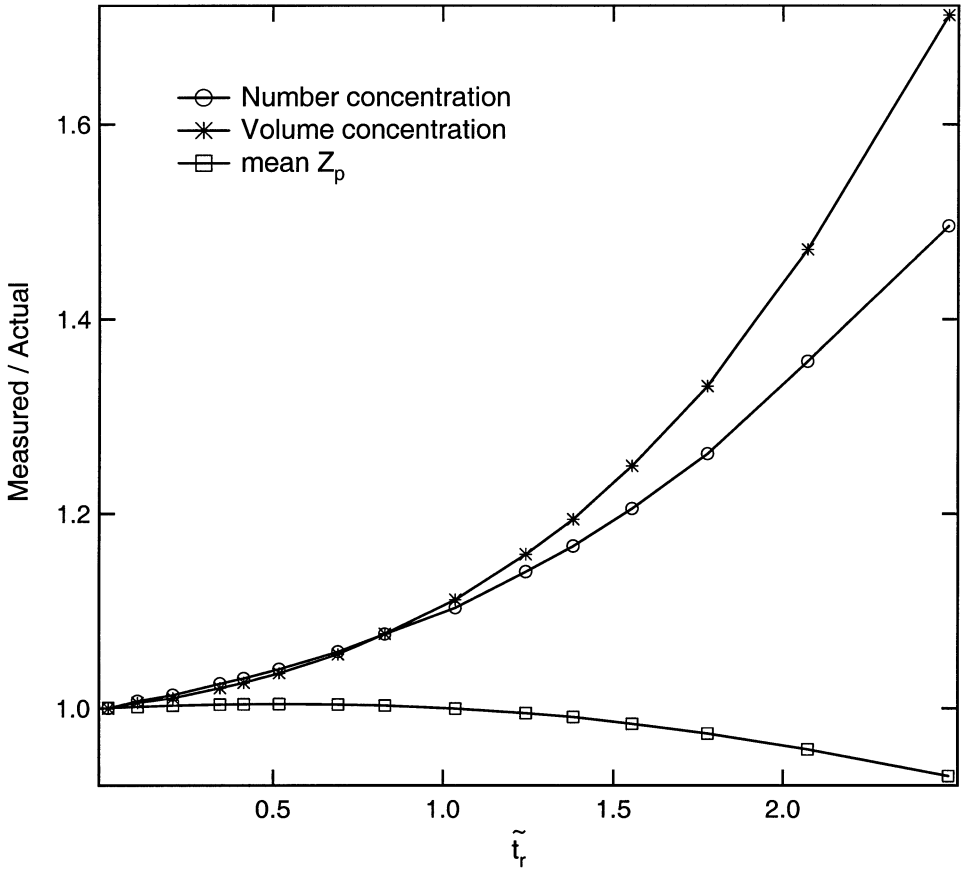

Figure 12. Expected concentration and mobility errors in recovered size distributions if the fixed voltage transfer function is used in the data inversion and the PSL approach is used to determine the plumbing time.

There are several possible approaches to correcting the mobility array corresponding to the counting intervals during a voltage scan. Rather than providing multipliers for the up and down scan that would shift the Z_p array calculated using the gas residence time, the approach taken here is to provide a plumbing time offset, Δt_d, which, when added to the plumbing time determined through one of the approaches discussed above, will result in the correct assignment of mobility to the counts bins. Since the residence time and electric field history for a classified particle is different during the up and down scans, two plumbing time offsets are needed. Rather than requiring that the mean mobility or mode mobility be correct for the size distribution measured, the approach taken here was to iteratively adjust Δt_d until the bias in recovered volume concentration was equal to that in recovered number concentration.

To apply these corrections to instruments for which the true transit time between the DMA outlet and detection point is known, plumbing time offsets for the up and down scan can be calculated for a given $\tilde{t}_r$. The sum of these offsets and the true transit time should then be used as the plumbing times. If the PSL approach is used to determine the appropriate plumbing time at one $\tilde{t}_r$ these offsets can be used to calculate the plumbing time for different ramp parameters. Offsets used to adjust the plumbing time determined using the UDA approach will roughly shift both the up- and down-scan distributions by an equal amount in the same direction. These UDA offsets represent the difference between the plumbing times calculated by matching the up- and down-scan distributions and those calculated by independently shifting each distribution until the number and volume concentration biases are the same. The coefficients for polynomial fits of the offsets of the forms given in Equations (7) and (8) are provided for both sets of offsets in Table 3. The calculated offsets

Table 3
Best-fit parameters for concentration and plumbing time corrections for $Q_{sh}/Q_a = 10$

	Up scan	Down scan
a_1	0.0139	0.0471
a_2	0.125	−0.1234
a_3	−0.9909	−0.9951
b_1	−0.0145	0.0211
b_2	0.1256	−0.1299
c_1	0.0664	0.0301
c_2	0.0329	−0.0506

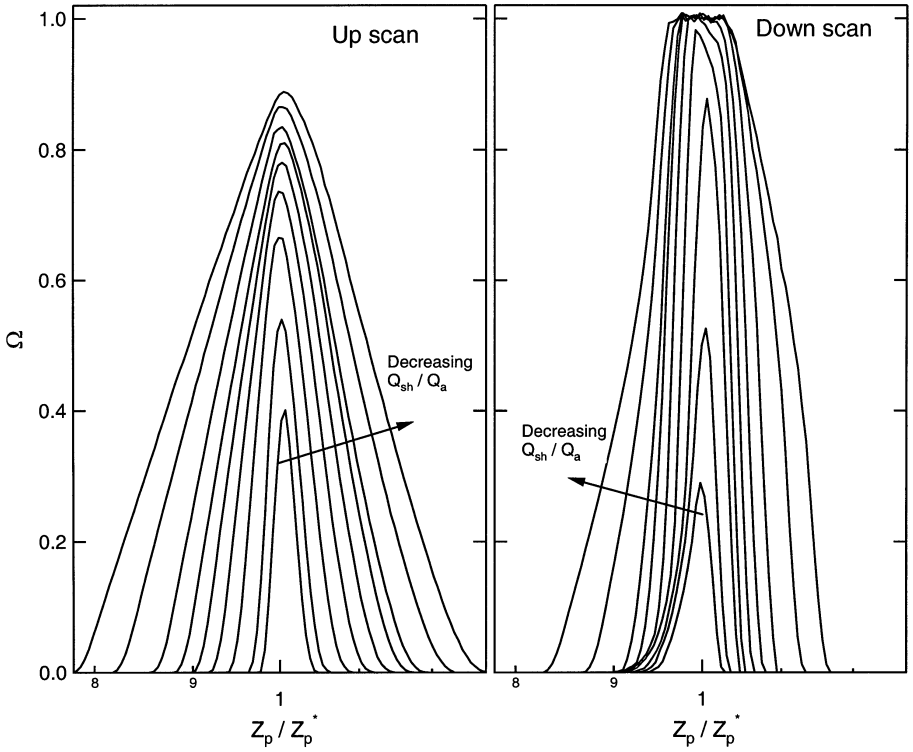

Figure 13. Simulated scanning DMA transfer functions for $Q_{sh} = 2.5$ l/min, $V_{\max}/V_{\min} = 1000$, $t_s = 60$ s, and $0.025 \leq Q_a \leq 0.5$ l/min.

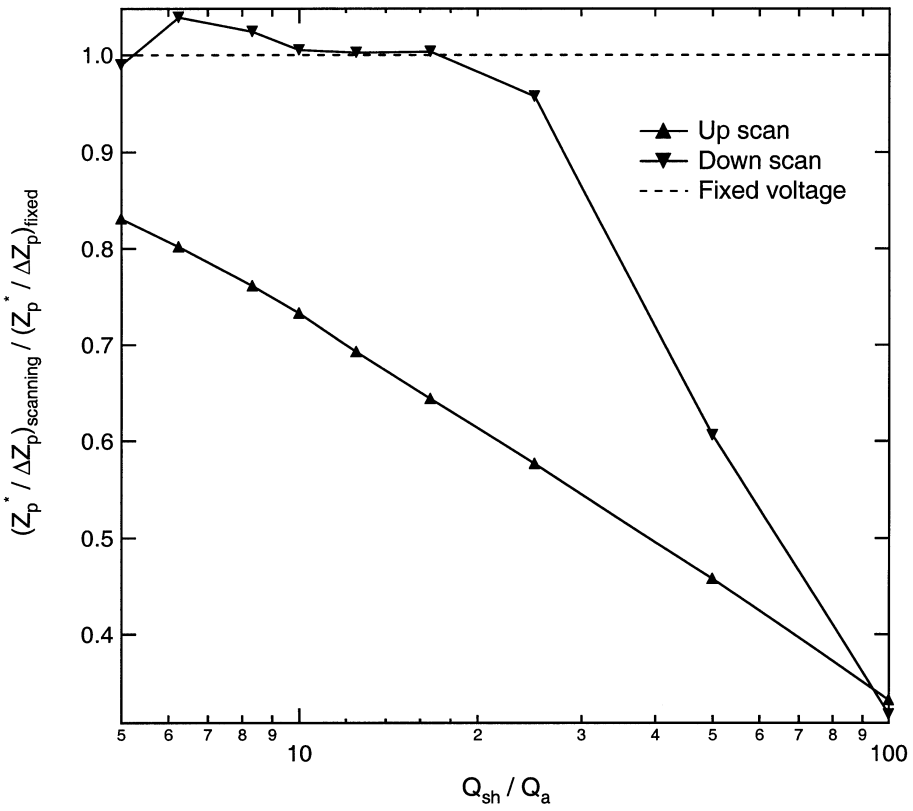

Figure 14. Simulated scanning DMA resolution normalized with respect to that for fixed voltage operation at the same Q_{sh}/Q_a flow ratio. The spacing between consecutive mobilities used in the simulations limits the smoothness of the curves.

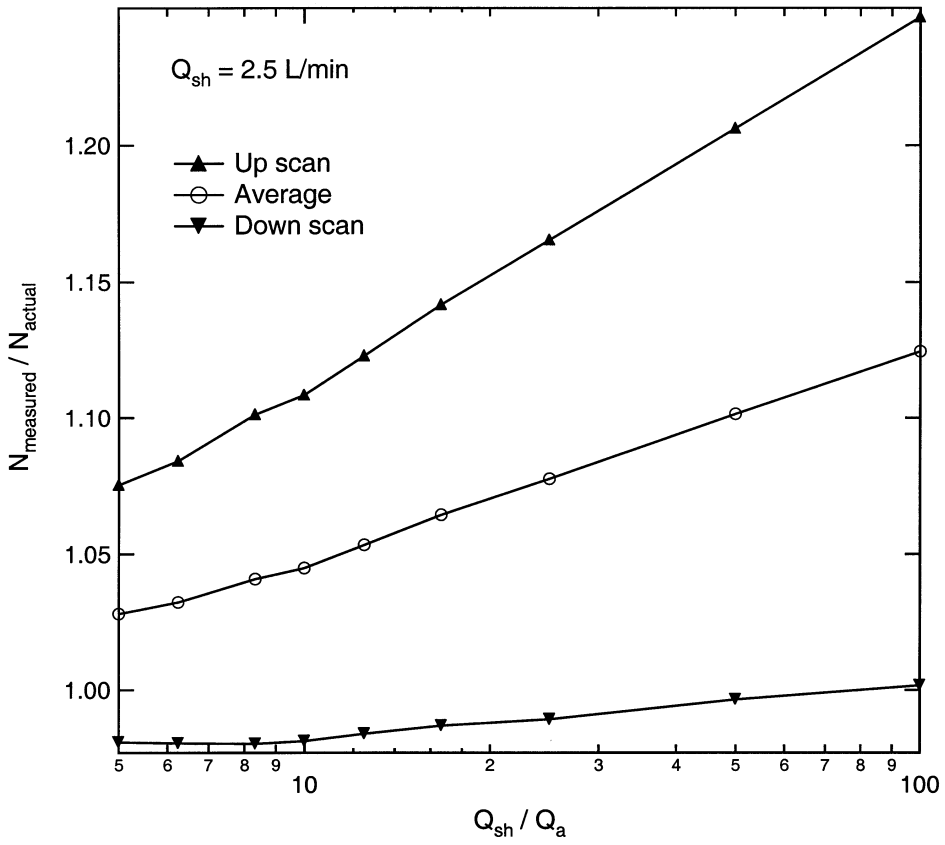

Figure 15. Expected concentration errors in recovered size distributions if the fixed voltage transfer function is used in the data inversion for measurements made with varying sheath-to-aerosol flow ratio.

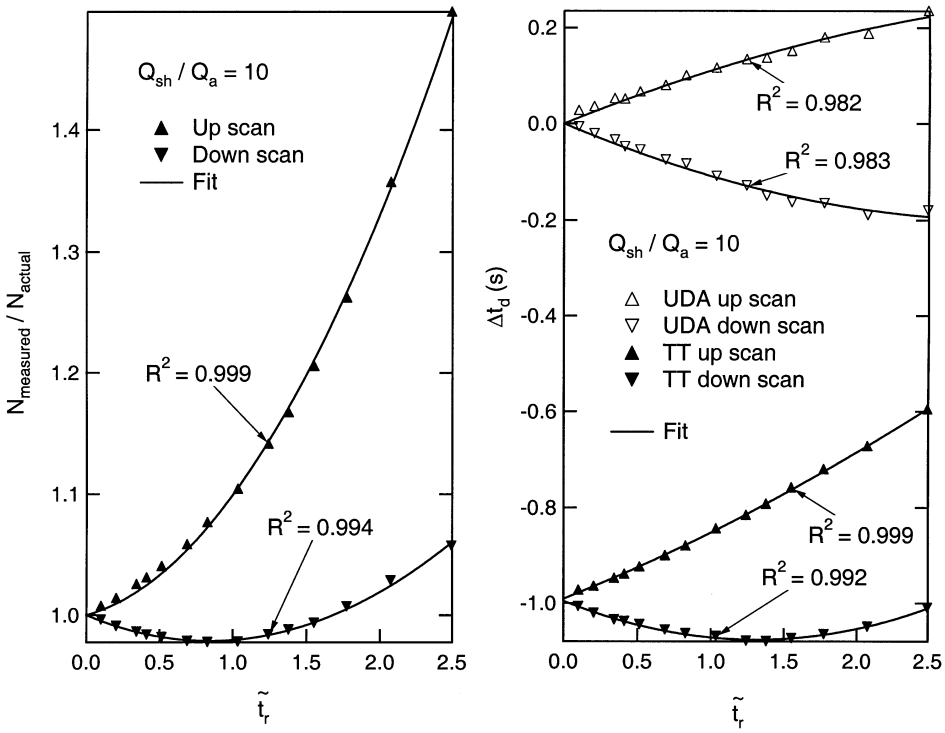

Figure 16. Plumbing time and concentration corrections that can be applied in conjunction with the fixed-voltage transfer function. These corrections apply to $Q_{sh} = 2.5$ l/min.

and best-fit curves are shown in Figure 16. These offsets were calculated only for a sheath-to-aerosol flow ratio of 10:

$$t_d(s) = (t_d)_{TT} + (\Delta t_d)_{TT} = (t_d)_{TT} + \frac{2.5s \cdot 1/\text{min}}{Q_{sh}}[a_1(\tilde{t}_r)^2 + a_2(\tilde{t}_r) + a_3], \quad [7]$$

$$t_d(s) = (t_d)_{UDA} + (\Delta t_d)_{UDA} = (t_d)_{UDA} + \frac{2.5s \cdot 1/\text{min}}{Q_{sh}}[b_1(\tilde{t}_r)^2 + b_2(\tilde{t}_r)]. \quad [8]$$

Following the adjustment of the mobility array, the impact of the differing area beneath the transfer functions can be accounted for by applying a concentration correction. These corrections were calculated in the same manner and using the same assumed log-normal size distribution as the concentration biases shown in Figures 9, 11, and 12 after the correct plumbing time offset was applied. As with the simulations that produced Figures 9, 11, and 12, these corrections are largely insensitive to the log-normal distribution used. The corrections were also fitted to polynomial expressions of the form given in Equation (9). These fitted curves are shown in Figure 16, and the parameters describing them are provided in Table 3:

$$\left(\frac{dN}{d\log D_p}\right)_{\text{corrected}} = \frac{\left(\frac{dN}{d\log D_p}\right)_{\text{original}}}{\left(\frac{N_{\text{measured}}}{N_{\text{actual}}}\right)} = \frac{\left(\frac{dN}{d\log D_p}\right)_{\text{original}}}{c_1(\tilde{t}_r)^2 + c_2(\tilde{t}_r) + 1}. \quad [9]$$

CONCLUSIONS

Unlike the symmetric and easily calculated transfer function for a fixed voltage DMA, scanning DMA transfer functions have an irregular shape that is difficult to parameterize. Even for aerosol size distributions that are broad relative to the width of the transfer function, the influence of this distortion is reflected in size and concentration biases. The errors caused by use of the fixed voltage transfer function increase with the ratio of the mean gas residence time to the exponential voltage time constant. One approach for minimizing these errors is to simply use long scan times. Alternatively, corrections such as those provided here can be applied in conjunction with the fixed voltage transfer function. Although the analysis here was limited to the TSI 3081 cylindrical DMA, similar results were found for DMAs with different dimensions, and even different geometries (i.e., radial). Unfortunately, the simulated transfer functions and their impacts on recovered distributions are themselves only approximations, since the influence of deviations from predicted velocity and electric field profiles has been neglected. Inclusion of these nonidealities would increase the accuracy of the predicted transfer functions but would also increase the complexity of the computations.

REFERENCES

Chen, D. R., Pui, D. Y. H., Mulholland, G. W., and Fernandez, M. (1999). Design and Testing of an Aerosol Sheath Inlet for High Resolution Measurements with a DMA, *J. Aerosol Sci.* 30:983–999.

Collins, D. R., Flagan, R. C., and Seinfeld, J. H. (2002). Improved Inversion of Scanning DMA Data, *Aerosol Sci. Technol.* 36:1–9.

Collins, D. R., Nenes, A., Flagan, R. C., and Seinfeld, J. H. (2000). The Scanning Flow DMA, *J. Aerosol Sci.* 31:1129–1144.

Eichler, T., De Juan, L., and De La Mora, J. F. (1998). Improvement of the Resolution of TSI's 3071 DMA Via Redesigned Sheath Air and Aerosol Inlets, *Aerosol Sci. Technol.* 29:39–49.

Endo, Y., Fukushima, N., Tashiro, S., and Kousaka, Y. (1997). Performance of a Scanning Differential Mobility Analyzer, *Aerosol Sci. Technol.* 26:43–50.

Fissan, H. J., Helsper, C., and Thielen, H. J. (1983). Determination of Particle Size Distributions by Means of an Electrostatic Classifier, *J. Aerosol Sci.* 14:S354–S357.

Hagwood, C., Sivathanu, Y., and Mulholland, G. (1999). The DMA Transfer Function with Brownian Motion a Trajectory/Monte-Carlo Approach, *Aerosol Sci. Technol.* 30:40–61.

Knutson, E. O., and Whitby, K. T. (1975). Aerosol Classification by Electric Mobility: Apparatus, Theory, and Applications, *J. Aerosol Sci.* 6:443–451.

Kousaka, Y., Okuyama, K., Adachi, M., and Mimura, T. (1986). Effect of Brownian Diffusion on Electrical Classification of Ultrafine Aerosol-Particles in Differential Mobility Analyzer, *J. Chemical Eng. Japan* 19:401–407.

Reischl, G. P., Makela, J. M., and Necid, J. (1997). Performance of Vienna Type Differential Mobility Analyzer at 1.2-20 Nanometer, *Aerosol Sci. Technol.* 27:651–672.

Russell, L. M., Flagan, R. C., and Seinfel, J. H. (1995). Asymmetric Instrument Response Resulting From Mixing Effects in Accelerated DMA-CPC Measurements, *Aerosol Sci. Technol.* 23:491–509.

Stolzenburg, M., Kreisberg, N., and Hering, S. (1998). Atmospheric Size Distributions Measured by Differential Mobility Optical Particle Size Spectrometry, *Aerosol Sci. Technol.* 29:402–418.

Stolzenburg, M. R. (1988). An Ultrafine Aerosol Size Distribution Measuring System. Ph.D. thesis, University of Minnesota, Minneapolis, MN.

Twomey, S. (1975). Comparison of Constrained Linear Inversion and an Iterative Nonlinear Algorithm Applied to Indirect Estimation of Particle-Size Distributions, *J. Comput. Phys.* 18:188–200.

Wang, S. C., and Flagan, R. C. (1990). Scanning Electrical Mobility Spectrometer, *Aerosol Sci. Technol.* 13:230–240.

Wiedensohler, A. (1988). An Approximation of the Bipolar Charge-Distribution for Particles in the Sub-Micron Size Range, *J. Aerosol Sci.* 19:387–389.

Winklmayr, W., Reischl, G. P., Lindner, A. O., and Berner, A. (1991). A New Electromobility Spectrometer for the Measurement of Aerosol Size Distributions in the Size Range From 1 to 1000 Nm, *J. Aerosol Sci.* 22:289–296.

Zhang, S. H., and Flagan, R. C. (1996). Resolution of the Radial Differential Mobility Analyzer for Ultrafine Particles, *J. Aerosol Sci.* 27:1179–1200.